

http://pubs.acs.org/journal/aesccq Article

# Sources and Dynamics of Submicron Aerosol during the Autumn Onset of the Air Pollution Season in Delhi, India

Kanan Patel, Sahil Bhandari, Shahzad Gani, Mark Joseph Campmier, Purushottam Kumar, Gazala Habib, Joshua Apte,\* and Lea Hildebrandt Ruiz\*



**Cite This:** *ACS Earth Space Chem.* 2021, 5, 118–128



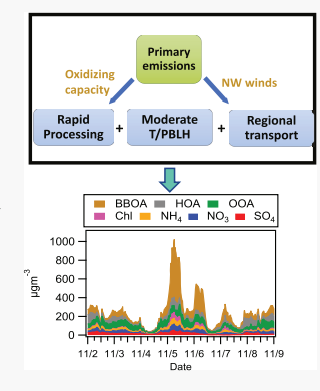
ACCESS

Metrics & More

Article Recommendations

Supporting Information

ABSTRACT: New Delhi, India is the most polluted megacity in the world and routinely experiences high particulate matter (PM) concentrations. As part of the Delhi Aerosol Supersite Study, we have been measuring PM<sub>1</sub> concentration and composition in Delhi continuously since January 2017. This paper focuses on autumn, one of the most polluted seasons in Delhi when PM<sub>1</sub> concentrations steadily increase throughout the season and can exceed  $1000~\mu g$  m<sup>-3</sup> during episodic events. Positive matrix factorization on the organic aerosol (OA) spectrum suggests comparable seasonal average contributions from hydrocarbon-like OA (HOA), biomass burning OA (BBOA), and oxidized OA (OOA), with BBOA dominating during episodic events. We demonstrate the influence of regional sources such as agricultural burning during this season through temporal trends of pollutants, PMF factors, meteorology, and nonparametric wind regression analysis. We use inorganic fragment ratios to show the influence of metals during the festival of Diwali. Furthermore, we demonstrate the influence of transitioning meteorology in governing PM<sub>1</sub> composition through the season. Overall, our analysis provides novel insights into the factors controlling PM<sub>1</sub> during one of the most polluted seasons in Delhi



KEYWORDS: Delhi, autumn, air pollution, particulate matter, aerosol chemical speciation monitor, positive matrix factorization

#### 1. INTRODUCTION

Exposure to fine particulate matter (PM) is a major risk factor for cardiovascular, respiratory, and other diseases. <sup>1–5</sup> Globally, outdoor PM<sub>2.5</sub> (PM of size <2.5  $\mu$ m) resulted in 4.2 million premature deaths in 2016, predominantly in low- and middle-income countries. In India, exposure to PM<sub>2.5</sub> has been estimated to reduce the average life expectancy by ~1.5 years, compared to ~0.4 years in the United States. Delhi, India is the second most populated megacity in the world (current population 28 million) and routinely experiences high air pollution levels, thereby making it a high-risk location for exposure to PM and associated adverse health effects. <sup>7,9–11</sup>

Atmospheric PM can originate from a range of natural and anthropogenic sources. 12,13 Primary aerosols are directly emitted, whereas secondary aerosols are formed from gaseous precursors via atmospheric oxidation and subsequent partitioning to the aerosol phase. 13–15 The atmospheric fate and concentration of ambient PM depends on numerous factors including primary emissions, meteorological factors (wind speed, direction, temperature, relative humidity, planetary boundary layer height), and the atmospheric oxidizing capacity. 16–23

Local sources of primary PM in Delhi include transportation, domestic biomass and trash burning, cooking, and industrial and construction activities.<sup>24–30</sup> Delhi is also downwind of many agricultural states such as Punjab and Haryana, which can be a source of PM from agricultural burning.<sup>31–35</sup> Further,

Delhi experiences cool winters with shallow boundary layer heights and frequent temperature inversions, which trap pollutants within the boundary layer causing especially polluted conditions. Rapid photochemical processing in Delhi contributes to the importance of secondary pollutants. Delhi contributes to the importance of secondary pollutants.

Autumn (mid-September–November) is an especially important transitional period in air quality in Delhi and across North India. During autumn, PM concentrations rapidly increase from their annual monsoon minima (June–August, typical levels  $30-50~\mu g~m^{-3}~PM_{2.5}$ ) to reach daily levels above  $200~\mu g~m^{-3}~PM_{2.5}$  and episodic high concentrations in excess of  $500-1000~\mu g~m^{-3}$ . While the sources, atmospheric dynamics, and chemistry of aerosols in Delhi have received sustained attention in recent years, we provide here new perspectives with a detailed investigation of the mechanisms driving the rapid increase in particle-phase pollution during autumn months.

Several features of the ambient aerosol in Delhi during autumn months merit brief introduction.<sup>31,32</sup> A few important seasonal sources of pollution are especially active during

Received: December 10, 2020 Revised: December 17, 2020 Accepted: December 18, 2020 Published: January 5, 2021





autumn months: a few weeks of intensive burning of rice ("paddy") crop stubble in the upwind states of Punjab and Haryana; 33,40 the festivals of Dussehra and especially Diwali, which involve the burning of fireworks; 41,42 and the resumption of brick-making season in uncontrolled brick kilns after the end of monsoon rains. Further, this season observes a sharp transition in meteorology since it is between monsoon (July-mid-September), which is hot, humid, and has higher planetary boundary layer height and mostly southern winds, and winter (December-mid-February), which is cold and has lower planetary boundary layer height and mostly northwestern winds.<sup>32</sup> Transitioning meteorology likely contributes to variability in sources impacting the city (due to changing wind direction) and also changes particle concentrations due to thermodynamic (partitioning) effects. As shown in Figure S1, a rapid increase of  $\sim 20-30 \ \mu g \ m^{-3}$ week in autumn months is typical over the recent years of the observational record. In addition, large episodic spikes in pollution, sometimes but not always coincident with festival periods, are common. Here, we focus on autumn 2018, a representative recent example of autumn air pollution for which we made intensive measurements of chemical composition. As part of the Delhi Aerosol Supersite study, we have been measuring the submicron aerosol composition, concentration, and size distribution using a suite of online instrumentation since January 2017.

The main objectives of our analyses are to understand factors contributing to the high concentrations observed in autumn 2018 by (1) interpreting the temporal trends in submicron composition and concentration, (2) using positive matrix factorization (PMF) to understand the nature and sources of organic aerosol (OA), and (3) interpreting the influence of meteorological parameters.

### 2. METHODS

2.1. Sampling Site, Instrumentation, and Data **Processing.** The Delhi Aerosol Supersite is located at the Indian Institute of Technology Delhi (IITD) campus in South Delhi. Details on the sampling site, instrumentation, and set up can be found in Gani et al., 2019.<sup>32</sup> Briefly, the bulk composition of nonrefractory PM<sub>1</sub> (NR-PM<sub>1</sub>) is measured using an Aerodyne Aerosol Chemical Speciation Monitor (ACSM, Aerodyne Research, Billerica MA).<sup>43</sup> Details on ACSM calibration are presented in Section S1 of the Supporting Information (SI). Black carbon (BC, at 880 nm), ultraviolet absorbing particulate matter (UV-PM, at 370 nm), and their difference (deltaC) are measured using a multichannel aethalometer (Magee Scientific Model AE33, Berkeley, CA). 44 Particle size distributions (PSD) are measured using a scanning mobility particle sizer (SMPS, TSI, Shoreview, MN). The SMPS was not operational during the Diwali period from November 4 to 8.

The SMPS scanned from 12 to 560 nm, and we used a mode fitting algorithm in the mass domain to estimate the PSD between 560 and 1000 nm. Although the ACSM recorded data every  $\sim\!1$  min, it was postaveraged to 15 points ( $\sim\!15$  min) for performing PMF and 60 min for comparison with SMPS data. Further details on ACSM data processing are presented in Section S1. The biomass burning and fossil fuel fractions of BC (BCbb and BCff respectively) were computed using the model of Sandradewi et al.

**2.2. Source Apportionment.** Positive matrix factorization (PMF) is a receptor modeling tool that has been widely used

in combination with ambient aerosol mass spectrometry data to apportion "factors" that serve as proxies for various PM sources and types. 47–56 The factors resolved usually correspond to emissions from primary sources including hydrocarbon-like OA, "HOA", used as a proxy for traffic emissions and biomass burning OA, "BBOA," used as a proxy for biomass burning emissions. OA formed from secondary reactions, secondary organic aerosol (SOA) is typically resolved as oxidized OA, "OOA". 19,31,47 Further separation of factors corresponding to sources such as cooking, coal combustion, trash burning, etc. may be possible depending on their contribution to total OA, correlation to other sources, as well as the mass resolution of the instrument. 25,47,48,57–60

We performed PMF on OA mass spectral data from the ACSM, utilizing the PMF Evaluation Tool, PET, <sup>47</sup> which uses the PMF2 algorithm. <sup>61</sup> We selected m/z 12–120 in the OA mass spectra due to a low signal-to-noise ratio at higher m/z. <sup>50,62</sup> We assigned physical meaning to the factors based on the abundance of specific m/z in their spectra, correlation with reference spectra <sup>47,63</sup> as well as with the time series of external tracers (e.g., CO, NO<sub>x</sub>, BC<sub>ff</sub>, BC<sub>bb</sub>, deltaC) where possible. <sup>47</sup> A three-factor solution was chosen to best represent the data as discussed further in Section 3.2. A value of zero was chosen for SEED and FPEAK because nonzero values either had no significant effect on the solution or led to unreasonable factors. Further details on the PMF runs and number of factors, SEED, and FPEAK scenarios are presented in Section S2 (Table S1, Figure S2).

**2.3. Other Data.** We retrieved data on hourly wind speed, wind direction (10 m above ground level), and planetary boundary layer height (H) from the NASA meteorological reanalysis data set MERRA2<sup>64</sup> and data on temperature and relative humidity from the Indira Gandhi International Airport (~8 km west of our site). We obtained daily fire counts in north India from the NASA fire information for resource management system (FIRMS) using the moderate resolution imaging spectroradiometer (MODIS, collection 6) data, <sup>65–67</sup> CO, NO<sub>x</sub>, and PM<sub>2.5</sub> data from the Central Pollution Control Board (CPCB) Central Control Room web interface (CCR) with additional processing steps summarized in Section S1.

We performed nonparametric wind regression analysis using ZeFir v3.7 $^{68}$  to identify potential source origins of the PM<sub>1</sub> species and the PMF factors. Briefly speaking, this is a source-to-receptor apportionment model that uses nonparametric kernel smoothing methods to apportion the observed concentrations to sectors defined by wind speed and wind direction. In order words, it estimates the concentration measured by the instrument as a function of wind speed and direction (the sources sampled depend on wind direction). Further details about the method are presented in Section S3.

#### 3. RESULTS AND DISCUSSION

**3.1. Temporal Trends in PM**<sub>1</sub> and Meteorological Parameters. The average C-PM<sub>1</sub> (NR-PM<sub>1</sub> + BC) concentration gradually increased from  $\sim 65~\mu g m^{-3}$  (averaged for the last two weeks) in September to  $\sim 220~\mu g m^{-3}$  in November (averaged for the whole month). The maximum hourly concentration of the study ( $\sim 1000~\mu g m^{-3}$ ) was observed during the early morning hours ( $\sim 06:00~a.m.$ ) of November 5 (Figure 2). The C-PM<sub>1</sub> concentration averaged for the entire season was 161  $\mu g m^{-3}$  (Table S2), higher than the concentrations observed in spring, summer, and monsoon and  $\sim 20\%$  lower than that observed in winter (diurnal

variation of average concentration/composition across all seasons is shown in Figure S3),<sup>32</sup> which experiences lower temperatures, boundary layer height, and likely more local emissions from domestic heating.<sup>30</sup>

As shown in Figure 1a (weekly moving average), the overall increase in  $C-PM_1$  through the season was accompanied by a

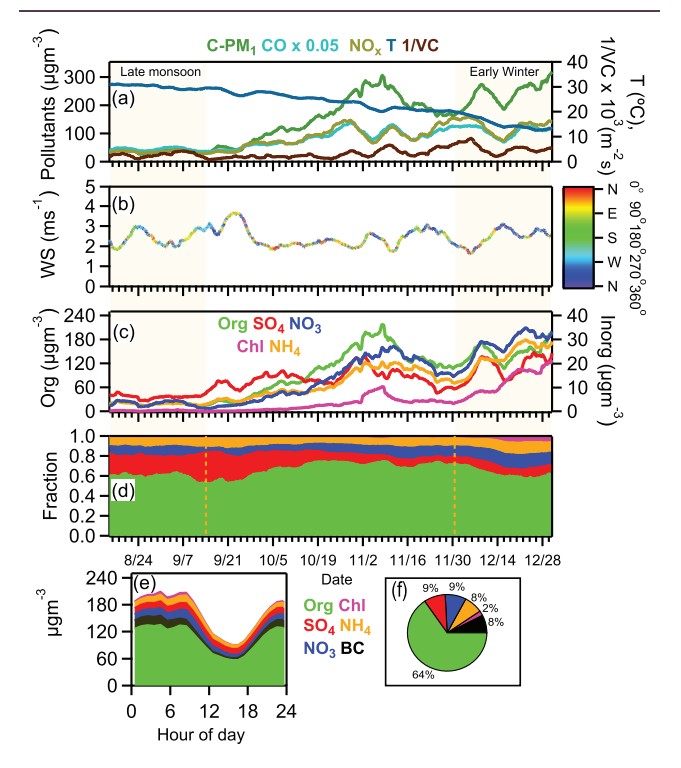


**Figure 1.** Weekly moving averages of (a) C-PM<sub>1</sub> (=NR-PM<sub>1</sub> + BC), CO, NO<sub>x</sub>, temperature, and the inverse of ventilation coefficient (VC = planetary boundary layer height  $\times$  wind speed); (b) wind speed (WS, colors represent the wind direction); (c) NR-PM<sub>1</sub> species concentrations; (d) NR-PM<sub>1</sub> composition; (e) average diurnal variation of C-PM<sub>1</sub> species; and (f) average C-PM<sub>1</sub> composition in autumn 2018.

decrease in average ventilation coefficient (VC = planetary boundary layer height  $\times$  wind speed) and temperature (T). Further, concentrations of NO $_x$  and CO (which are mostly associated with local sources) varied with 1/VC while C-PM $_1$  increased consistently and rapidly until mid-Nov, indicating the impact of additional sources such as regional PM.

Figure 1c,d show the weekly moving averages of the NR-PM<sub>1</sub> species concentrations and composition, respectively, through late monsoon, autumn, and early winter. Sulfate (SO<sub>4</sub><sup>2-</sup>) concentration was initially higher than the other inorganic species but was outcompeted by nitrate (NO<sub>3</sub><sup>-</sup>) and ammonium (NH<sub>4</sub><sup>+</sup>) by November. Since sulfate is nonvolatile, its concentration is not expected to be influenced by changes in temperature. On the other hand, ammonium nitrate (NH<sub>4</sub>NO<sub>3</sub>) is semi-volatile and partitions to the particle phase at lower temperatures. The increase in chloride (Cl<sup>-</sup>) concentration was more significant in (early) winter than autumn, consistent with further reduction in temperature and the volatile nature of ammonium chloride (NH<sub>4</sub>Cl).<sup>70</sup> Thus, the increase in  $NH_{4,}^{+}NO_{3}^{-}$ , and  $Cl^{-}$  concentrations in autumn was likely driven by VC and temperature, while the increase in SO<sub>4</sub><sup>2-</sup> concentration was driven mainly by VC. Further, the largest increase in concentration in autumn was observed in

organics, pointing to the role of increased diversity of sources during this season. Overall, the fraction of  ${\rm SO_4}^{2-}$  decreased, and the fraction of organics and  ${\rm NO_3}^-$  increased through autumn (Figure 1d). In early winter (December 1–31), the organic fraction decreased as  ${\rm NO_3}^-$  and  ${\rm Cl}^-$  fractions increased further, reflective of differences in composition in autumn versus winter.

The average organic fraction in C-PM $_1$  in autumn 2018 was  $\sim$ 64% (Figure 1f), higher than other seasons (where it was less than or equal to  $\sim$ 55%),  $^{32}$  indicating that the source mixture in autumn is different than in other seasons (Figure S3). As shown in Figure 1e, OA peaked during the morning hours between 07:00 and 09:00 a.m. and during the nighttime hours between 09:00 and 11:00 p.m., due to the influence of local emissions (such as traffic and local biomass burning). Interestingly, unlike other seasons which observed a dip in OA concentration during the early morning hours (Figure S3), the OA concentration in autumn remained relatively constant through 00:00–7:00 a.m., suggestive of the influence of additional sources during those hours.

Overall, the hourly averaged C-PM<sub>1</sub> data compared well with the SMPS PM<sub>1</sub> estimate (Figure S4;  $R^2 = 0.91$ ). It also compared reasonably well with the regulatory monitor-based PM<sub>2.5</sub> data (Figure S5) on most days except the period from November 7 to 9. On the night of Diwali (November 7), the maximum C-PM<sub>1</sub> concentration (~230  $\mu$ g m<sup>-3</sup>) was not as high as the concentrations observed on the earlier days (Figure 2). Although PM<sub>2.5</sub> monitoring sites recorded peaks on/after

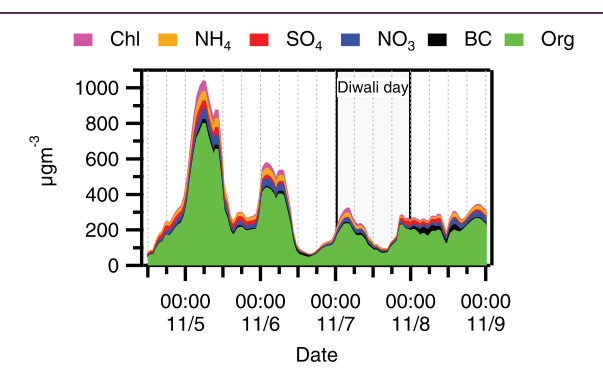


Figure 2. High-concentration episode from November 4 to 8, 2018 (hourly averages are shown).

the Diwali day, there were differences in the peak concentration values as well as the time at which they were observed (see a temporal trend in Figure S6b). Meteorological data during the period indicate a change in wind direction from North West to North East/South East and slower winds starting November 7 (Figure S6a). Thus, the lower concentration measured on the night of Diwali might have been due to the instrument sampling a different local plume as a result of the relatively stagnant wind conditions and the absence of high emission sources in the proximity of our site located inside the IIT-Delhi campus. Further, fireworks emit mineral dust and metals which are not detected by the ACSM.<sup>71</sup> We observed some evidence of metal compounds during Diwali, as discussed in Section 3.3. Furthermore, previous studies have found that a large fraction of PM from fireworks may be larger than 1  $\mu$ m, <sup>71</sup> which would not have been sampled by the ACSM. Additionally, there was an influence of agricultural burning on the earlier days considering that the winds were faster and from the north west direction, a

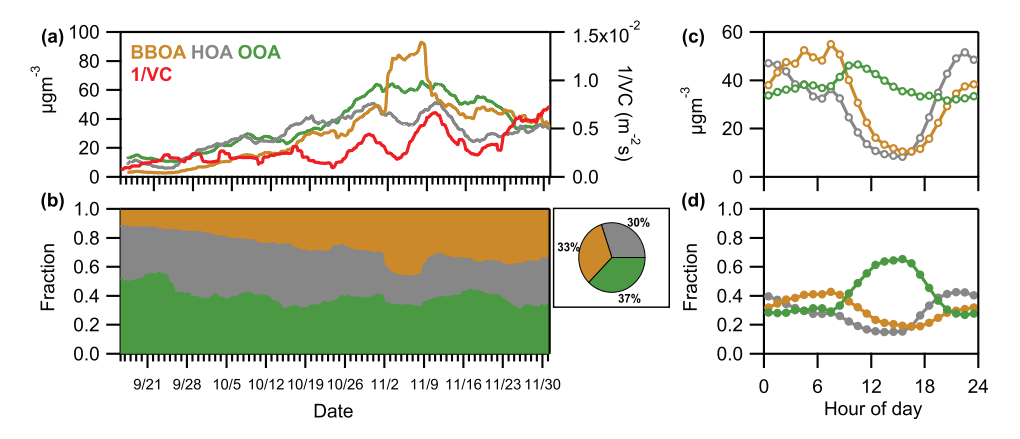


Figure 3. (a) Weekly moving averages of PMF factor concentrations. The inverse of ventilation coefficient (VC = planetary boundary layer height  $\times$  wind speed) has been added to track the change in meteorology. (b) Weekly moving averages of PMF factor fractions. The pie chart depicts the average OA composition. Average diurnal variations in factor concentrations and fractions are depicted in (c) and (d), respectively.

topic we discuss further in Sections 3.2 and 3.4. Thus, we did not observe such high concentrations on Diwali because of meteorology, as well as the limitations of the ACSM in measuring metals, dust, and particles of size greater than 1  $\mu$ m.

The average particle number (PN) concentration in autumn 2018 (39 000 cm<sup>-3</sup>; Table S2) was comparable to that observed in autumn 2017 (38 000 cm<sup>-3</sup>).<sup>72</sup> Further, the diurnal variation in particle number and mass concentrations (Figure S7) of nucleation (sub-25 nm), Aitken (25–100 nm), and accumulation (100–1000 nm) modes compared remarkably well between the two periods, indicating little interannual variation in the sources and processes governing these modes, and suggesting that our data for autumn 2018 is representative of autumns in Delhi.

3.2. Insights from Source Apportionment. PMF performed on OA for this season resolved three factors two primary factors, HOA and BBOA, and a secondary factor, OOA, which were identified based on their correlation with reference factors (Pearson R > 0.9), and external tracers (Figures S8 and S9). Intense and sporadic events (e.g., fireworks, intense wood burning, etc.) can influence the PMF results and are therefore usually excluded when running the model.<sup>73,74</sup> We tested the influence of high-concentration episodes observed from November 4 to 8 on our results by running a PMF model with the exclusion of that period. The resulting factors' mass spectra and time series were highly correlated with the PMF results obtained for the whole period (Pearson R = 0.99; Figures S8 and S9), and the slopes of the scatter plots of the respective PMF factor concentrations were close to 1 (Figure S10). Thus, these high-concentration episodes had little impact on the overall results, and we therefore use results from PMF performed on the whole period for the discussion below.

3.2.1. Factor Mass Spectra. The mass spectra (MS) of HOA has increased signals at m/z 41, 43, 55, 57, 69, 71, etc., usually corresponding to the fragments of aliphatic hydrocarbons ( $C_nH_{2n-1}$  and  $C_nH_{2n+1}$ ) resulting from traffic emissions (Figure S11a). It is highly correlated with the HOA MS obtained in spring 2018 (Pearson R = 0.99; Figure S12a), suggesting a consistent signature of this source (BBOA and HOA separation was achieved only in spring 2018 of our previous analysis<sup>31</sup>). A relatively high ratio of m/z 55/57 ( $\sim$ 1.23, compared to  $\sim$ 1.05 in reference HOA) suggests the potential influence of cooking organic aerosol (COA) on this

factor.  $^{53,58,62,75-77}$  However, the enhancement is lower than that in the reference COA factor (~2.92; Figure S12b), indicating that it was a minor contributor. This is aborton consistent with the plot of  $f_{55}$  (fraction of OA mass at m/z 55) versus  $f_{57}$  in a triangle plot  $^{78}$  (Figure S12c), where most of the points in autumn 2018 lie close to the HOA line(s), indicative of minor contribution from COA. The time series (TS) of HOA is correlated with the external tracers for traffic emissions, CO, NO<sub>x</sub>, BC, and BC<sub>ff</sub> (Figure S8a).

BBOA MS has enhanced signals at m/z 29, 60, and 73 (Figure S11b), usually associated with the fragments CHO+, C<sub>2</sub>H<sub>4</sub>O<sub>2</sub><sup>+</sup>, and C<sub>3</sub>H<sub>5</sub>O<sub>2</sub><sup>+</sup>, respectively, resulting from anhydrous sugars such as levoglucosan. 57,79,80 Its MS is correlated with the BBOA MS obtained in spring 2018 (Pearson R = 0.9) with some differences including a higher  $f_{44}$  and  $f_{60}$  in autumn (Figure S13). Figure S14a depicts  $f_{44}$  versus  $f_{43}$  for autumn BBOA, its comparison with reference BBOA, as well as the profiles of fresh and aged (~5 h) rice/wheat OA from literature.81 The data points for autumn 2018 BBOA lie in between fresh and aged agricultural burning OA, indicating that it likely had contribution from regional (aged) as well as local (fresh) biomass burning sources. Further, Figure S14b shows that autumn 2018 BBOA has a higher  $f_{60}$  and  $f_{44}$  than the reference BBOA. Differences in  $f_{60}$  may be due to increased contribution from sources with higher levoglucosan content, 82 while a higher  $f_{44}$  points toward faster aging and/or contribution from regional sources.<sup>81</sup> The autumn BBOA TS is correlated with the external tracers for biomass burning such as deltaC and BC<sub>bb</sub> (Figure S8b). It is also correlated with chloride (Pearson R = 0.95), indicating that the chloride during this season was likely associated with biomass burning (also see Sections 3.3 and 3.4). We compared the average OA spectra of autumn and winter to get an understanding of the overall OA source mixture during the two periods since we were not able to resolve BBOA in the winter seasons previously analyzed.<sup>31</sup> Autumn OA is more oxidized than winter OA (higher  $f_{44}$ , Figure S15), pointing toward the role of increased photochemical processing and/or contribution from the regionally transported PM. The regional contribution is also suggested by the aethalometer data-high deltaC, and BBpercent values were observed in autumn and winter, indicating contribution from biomass burning during both periods (see temporal trend in Figure S16a). However, the compensation parameter values (Figure S16b; used to correct for spot loading effects), which are expected to be higher for fresher aerosols (close to the source) and lower for processed aerosols (away from the source)<sup>44</sup> were lower during the autumn period, indicating an increased influence of regional biomass burning sources on the deltaC observed during this season. This suggests that the BBOA in autumn has a higher contribution from regional agricultural biomass burning, whereas the BBOA in winter has a relatively higher contribution from domestic biomass burning.

The  $f_{44}$  signal in OOA (Figure S11c) is higher than the corresponding signal in the reference OOA spectrum (by a factor of ~1.4; Figure S17), similar to other seasons, suggestive of rapid photochemical processing of fresh emissions.<sup>31</sup>

3.2.2. Temporal Trends of PMF Factors. Concentrations of all factors increased through the season (Figure 3a), but the fractional increase in BBOA concentration was the largest, increasing not only with time (Figure 3b) but also with the concentration of NR-PM<sub>1</sub> (Figure S18b). The clear peak in BBOA concentrations during the first week of November suggests that the episodic events November 5 and 6 were due to increased biomass burning (15 min averaged data shown in Figure S18a). Furthermore, the variation in HOA concentration (which is associated with local sources such as traffic) anticorrelated with the variation in ventilation coefficient, indicating that its increase was mostly associated with changing meteorology. In contrast, the increase in BBOA, especially between mid-October and mid-November did not correlate strongly with the decrease in ventilation coefficient, pointing toward the influence of other sources. This increase in BBOA concentration was consistent with the increase in fire counts in northern India during the period (temporal trend of daily fire counts in Figure S19), indicating that regional agricultural fires contributed to BBOA during this period. The BBOA fraction remained high even when the fire counts dropped toward the end of November, presumably due to an increase in the contribution of BBOA sources such as domestic heating owing to the lower ambient temperatures (Figure 1).

In terms of diurnal variation in concentration (Figure 3c), HOA had morning (07:00-09:00 a.m.) and nighttime (09:00-11:00 p.m.) peaks corresponding to traffic hours, with the nighttime peak being larger than the daytime peak, likely due to the absence of photochemistry (which converts HOA to OOA) and some influence of cooking activities during those hours (Section 3.2.1). The dip in the primary OA (HOA and BBOA) factor concentrations during the afternoon hours was concurrent with the increase in planetary boundary layer height (H), temperature (see their diurnal variation in Figure S20), and photochemistry. BBOA concentration increased through the nighttime and early morning hours after the afternoon dip, indicative of BBOA source(s) during those hours, such as agricultural burning. The secondary factor, oxidized OA (OOA), observed a small daytime peak (08:00 a.m.-10:00 a.m.) but otherwise remained relatively constant through the day, consistent with photochemical formation mostly off-setting the effects of the increasing H during the afternoon.

In terms of diurnal variation in OA composition (Figure 3d), BBOA dominated during the early morning (02:00–08:00 a.m.), constituting  $\sim$ 37–43% of OA, while HOA dominated during the night (09:00 p.m.–01:00 a.m.), constituting  $\sim$ 39–41% of OA. OOA dominated during the day (09:00 a.m.–08:00 p.m.), constituting 41–65% of OA, consistent with daytime photochemistry being the main pathway for the

formation of oxygenated OA. In the triangle plot<sup>51</sup> of diurnally averaged  $f_{44}$  versus  $f_{43}$  (Figure S21b), all data points lie within the triangle, with the afternoon data points occupying the top left position. On average, all three factors had a comparable contribution to OA (HOA–30%, BBOA–33%, and OOA–37%), suggesting similar contributions of biomass burning (BBOA), traffic (HOA), and secondary OA (OOA) during this season (Figure 3b). Statistical metrics which indicate the influence of outliers (i.e., episodic events)—standard deviation, arithmetic mean—median, and geometric standard deviation—are the highest for BBOA (Table S3), due to the influence of agricultural burning.

3.3. Insights from Inorganic Fragment Ratios. The enhancement in the ratio of  $NO_3^-$  fragments at m/z 30 ( $NO^+$ ) to m/z 46 (NO<sub>2</sub><sup>+</sup>) with respect to the value obtained for pure ammonium nitrate points toward the relative importance of organonitrates.<sup>83</sup> During the autumn season, the ratio decreased through the progression of the season as total particulate NO3 increased (see a temporal trend in Figure S22a), indicating that the relative contribution of organonitrates decreased through the season, likely a result of an increase in the inorganic nitrate fraction at lower temperatures (Figure 1). Interestingly, the NO<sup>+</sup>/NO<sub>2</sub><sup>+</sup> ratio started to increase on the night of November 7 (Diwali) and reached ~3 × calibration value (of that of ammonium nitrate) on the early hours of the following day (Figure S22b), likely due to the presence of metal nitrates such as sodium nitrate (NaNO<sub>3</sub>) and potassium nitrate (KNO<sub>3</sub>) in fireworks, <sup>84,85</sup> which have been shown to produce high NO<sup>+</sup>/NO<sub>2</sub><sup>+</sup> ratios. <sup>86</sup> Further, similar to the enhancement in NO<sup>+</sup>/NO<sub>2</sub><sup>+</sup>, an enhancement in  $SO^+/H_\nu SO_x^+$  and  $SO_2^+$   $/H_\nu SO_x^+$  was also observed (see a temporal trend in Figure S23) on the night of Diwali, likely due to the presence of metal sulfates in the fireworks.8

Quantification of potassium ( $K^+$ , m/z 39) using ACSM is challenging because of uncertainties in vaporization and surface ionization as well as interference of the organic fragment  $C_3H_3^+$  at m/z 39.88 The enhancement in the ratio of m/z 39 to 43 can be used to detect the presence of potassium  $(K^+)$ , since while m/z 39 can have large interferences from the organic fragment  $C_3H_3^+$ , m/z 43 is completely organic. In autumn 2018, m/z 39 was highly correlated with m/z 43 (Pearson R = 0.99; Figure S24a), indicating that the fragment was mostly organic. However, an enhancement in m/z 39/43 (over the baseline ratio) was observed during the Diwali period, i.e., November 7-8 and on November 4 (see a temporal trend in Figure S24b) indicative of the presence of K<sup>+</sup> during these periods. It was likely present during the other periods too given the influence of biomass burning during this season (and the association of K+ with biomass burning emissions 24,89,90) but could not be separated from the organic contribution at m/z 39.

The correlation between m/z 36 (HCl<sup>+</sup>) signal and organics mass may indicate the presence of organic chloride. However, this method may not be applicable if there are sources that emit organics along with inorganic chloride. In autumn 2018, m/z 36 signal was correlated with organics (Pearson R=0.86; Figure S25a), but the season experienced sources such as biomass burning (BBOA) and fireworks (Sections 3.1 and 3.2) which are known to emit inorganic chloride, e.g., chlorine that may be associated with ammonium and/or potassium from biomass burning, as seen in Nepal during the NAMaSTE study,  $^{92,93}$  and other studies around the world,  $^{94,95}$  or chlorine associated with potassium from

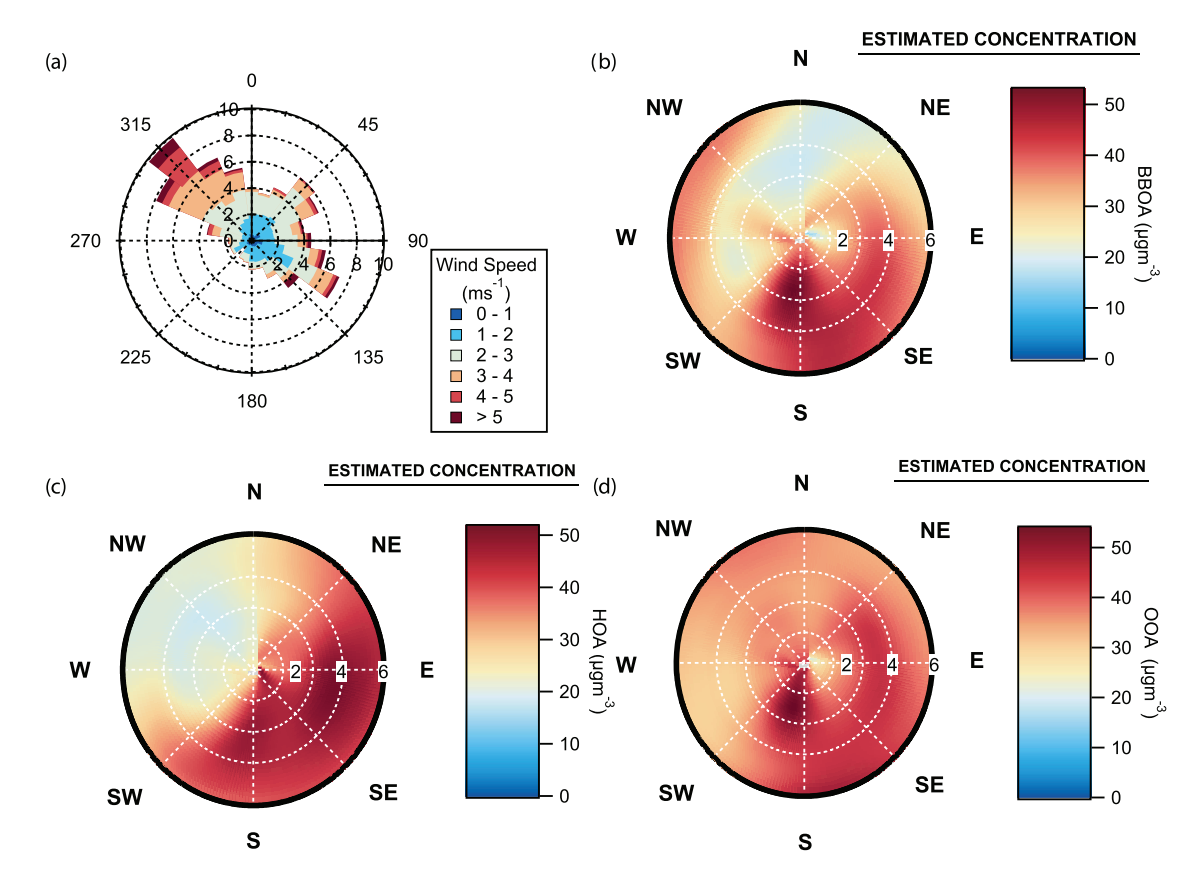


Figure 4. (a) Average wind rose for autumn 2018. The radial values correspond to % frequency. Nonparametric wind regression of (b) BBOA, (c) HOA, and (d) OOA. The radial values correspond to the wind speeds in ms<sup>-1</sup>.

fireworks.<sup>71</sup> During autumn 2018, chloride had a very high correlation with BBOA (Pearson R = 0.95; Figure S25b), indicating that it was associated with biomass burning, likely in both organic and inorganic forms, considering the evidence of  $K^{+}$  and a moderate correlation with  $NH_{4}^{+}$  (Pearson R = 0.75; Figure S25b). Ammonia (NH<sub>3</sub>) may be emitted from sources other than biomass burning but can neutralize HCl associated with biomass burning to form particulate ammonium chloride (NH<sub>4</sub>Cl). 92,93 Further, similar to BBOA, the average chloride fraction increased with increasing NR-PM<sub>1</sub> (see scatter plot in Figure S26). Furthermore, a comparison of normalized weekly moving averages of the PMF factors and inorganic species (Figure S27; normalized to the average concentration observed in the last two weeks of September) indicates that while concentrations of all species increased with the onset of autumn, the increases in chloride and BBOA were most notable (both increased by a factor of 20-30) and correlated with each other. These observations are consistent with the concurrent emissions of organic aerosol and chloride from biomass burning as also observed in other studies.9

**3.4. Insights from Meteorological Data.** We used nonparametric wind regression analysis to understand the influence of wind speed and direction. We tested the statistical significance of the correlations of average concentrations with meteorological parameters (see scatter plots in Figures S28 and S29) using a significance level of 0.05 (i.e., a p-value < 0.05 indicates that the correlation was statistically significant). The p-values and adjusted  $R^2$  for the correlation between different variables are presented in Tables S4 and S5 and are discussed below.

3.4.1. Wind Speed and Direction. As shown in the average wind rose (Figure 4a), autumn 2018 observed winds from north west, east, and south east. Further, on average, winds from northwest (NW) were relatively faster (>50% of wind speeds >3 ms<sup>-1</sup>). Nonparametric wind regression (Figure 4b) shows BBOA sources in the NW and S directions. The source in NW is likely agricultural burning from the northwestern states of Punjab and Haryana, considering the spread across the NW region at higher wind speeds (regional contributions are expected to increase with faster winds). On average, BBOA concentration decreased with an increase in wind speed (Figure S28a and Table S5), reflective of the contribution from "local" biomass burning sources (e.g., domestic heating), considering that local contributions are expected to decrease with an increase in wind speed. This observation is consistent with the BBOA MS, which saw contribution from local and regional sources, as discussed in Section 3.2.

For the HOA factor (Figure 4c), the sources are in E/SE, likely due to the proximity of the major roads of Aurobindo Marg and Outer Ring Road (see location in Figure S30). HOA is also inversely related to wind speed (Figure S28a), corroborating that it originated from local sources. The OOA concentration is distributed over different speed/wind directions in the NWR plot (Figure 4d), as expected from secondary OA. However, it is slightly inversely correlated with wind speed (Figure S28a and Table S5). This observation combined with a high oxidation state (Section 3.2) is consistent with rapid photochemical processing of emissions contributing to OOA. Among the nonorganic NR-PM<sub>1</sub> species (see NWR plots in Figure S31), the NWR plots of Cl<sup>-</sup> and

 $\mathrm{NH_4}^+$  are similar to BBOA, indicative of the association of  $\mathrm{Cl}^-$  with  $\mathrm{NH_4}^+$  and BBOA, in line with our findings in Section 3.3.  $\mathrm{SO_4}^{2-}$  concentration is spread across all directions and wind speeds, reflective of its regional nature.  $\mathrm{NO_3}^-$  observed higher concentrations from NW and S at lower wind speeds, reflective of the local nature of  $\mathrm{NO_x}$  pollution, which is associated with the formation of inorganic and organic nitrate, which constitute  $\mathrm{NO_3}^-$  observed in the ACSM.

3.4.2. Temperature, Relative Humidity, Planetary Boundary Layer Height, and Ventilation Coefficient. The concentrations of primary OA PMF factors (BBOA and HOA) decreased with increasing temperature (T), planetary boundary layer height (H), and ventilation coefficient (VC =wind speed × planetary boundary layer height) (Figure S28b,d,e and Table S5). The decrease with T is presumably due to the evaporation of semivolatile species at higher T; the decrease with H and VC is due to dilution. OOA concentrations did not have a statistically significant correlation with T or H, presumably due to a correlation between photochemistry and higher T and H, which would offset the effects of partitioning and dilution. With respect to relative humidity (RH), average HOA and BBOA increased up to RH ~ 75% and decreased afterwards (Figure S28c). This was likely due to the primary emission peaks coinciding with the time at which average RH was around 75% (Figure S20) and the influence of precipitation at high RH (>90%; such high RH values were observed mostly during the last two weeks of September which marks the end of monsoon season). Among the nonorganic NR-PM<sub>1</sub> species, average Cl<sup>-</sup>, NO<sub>3</sub><sup>-</sup>, and NH<sub>4</sub><sup>+</sup> concentrations decreased with increasing T, H, and VC (Figure S29b,d,e and Table S5).  $SO_4^{\ 2-}$  did not have a statistically significant correlation with any of these variables (Table S5), reflective of its nonvolatile and regional nature. With respect to RH, Cl<sup>-</sup>, NO<sub>3</sub><sup>-</sup>, and NH<sub>4</sub><sup>+</sup>concentrations increased with increasing RH and decreased at very high RH (>90%) likely due to precipitation (Figure S29c).  $SO_4^{2-}$  also increased with increasing RH, albeit to a lesser extent than the other species. This is consistent with other recent studies around the world 98,99 that have hypothesized the transformation of gaseous HNO3 and HCl into aqueous phase particles at high RH. Another reason could be that high RH usually coincides with low T, which facilitates increased partitioning of NO<sub>3</sub><sup>-</sup> and Cl<sup>-</sup> to particle phase.

Thus, temperature and ventilation played an important role in governing the primary OA species (HOA, BBOA) and the more volatile and local nonorganic NR-PM<sub>1</sub> species (Cl<sup>-</sup>, NH<sub>4</sub><sup>+</sup>, and NO<sub>3</sub><sup>-</sup>). Overall, primary emissions and their interplay with meteorology played a dominant role in influencing air pollution levels during one of the most polluted seasons in Delhi. Specifically, we observed that while HOA was mostly emitted from local sources (traffic), BBOA had contributions from regional agricultural burning in addition to local sources, as opposed to winter, which sees mostly local biomass burning sources. Further, particulate Cl<sup>-</sup> also had contributions from biomass burning sources. The Diwali period observed contributions from metals associated with fireworks. Future studies would benefit from mobile measurements using high-resolution instruments in the region to quantify and apportion the influence of regional versus local sources contributing to BBOA and PM1 during this season. From a policy perspective, it is evident that a combined effort at the state level (to control local sources) and central level (to

control regional sources such as agricultural burning) is necessary to control air pollution in the city.

#### ASSOCIATED CONTENT

## **3** Supporting Information

The Supporting Information is available free of charge at https://pubs.acs.org/doi/10.1021/acsearthspace-chem.0c00340.

Details on ACSM calibration and data processing (Section S1), PMF analysis (Section S2), nonparametric regression (Section S3), and 31 figures and 5 tables supporting the main paper (PDF)

### AUTHOR INFORMATION

## **Corresponding Authors**

Joshua Apte — Department of Civil and Environmental Engineering, University of California, Berkeley, Berkeley, California 94720, United States; School of Public Health, University of California, Berkeley, Berkeley, California 94720, United States; orcid.org/0000-0002-2796-3478; Email: apte@berkeley.edu

Lea Hildebrandt Ruiz — McKetta Department of Chemical Engineering, The University of Texas at Austin, Austin, Texas 78758, United States; orcid.org/0000-0001-8378-1882; Email: lhr@che.utexas.edu

#### **Authors**

Kanan Patel — McKetta Department of Chemical Engineering, The University of Texas at Austin, Austin, Texas 78758, United States; © orcid.org/0000-0002-2368-8624

Sahil Bhandari — McKetta Department of Chemical Engineering, The University of Texas at Austin, Austin, Texas 78758, United States

Shahzad Gani — Department of Civil, Architectural and Environmental Engineering, The University of Texas at Austin, Austin, Texas 78758, United States; Institute for Atmospheric and Earth System Research, University of Helsinki, Helsinki 00560, Finland; orcid.org/0000-0002-6966-0520

Mark Joseph Campmier – Department of Civil and Environmental Engineering, University of California, Berkeley, Berkeley, California 94720, United States

Purushottam Kumar — Department of Civil and Environmental Engineering, Virginia Polytechnic Institute and State University, Blacksburg, Virginia 24061-0131, United States; orcid.org/0000-0002-7692-095X

Gazala Habib — Department of Civil Engineering, Indian Institute of Technology Delhi, New Delhi 110016, India

Complete contact information is available at: https://pubs.acs.org/10.1021/acsearthspacechem.0c00340

#### Notes

The authors declare no competing financial interest.

## ■ ACKNOWLEDGMENTS

This paper is based on work supported by the Welch Foundation under grant no. F-1925-20170325 and F-1925-20200401 and the National Science Foundation under grant no. 1653625. Joshua S. Apte was supported by the Climate-Works Foundation. We thank the funding agencies for their support.

### **■** REFERENCES

- (1) Dockery, D. W.; Pope, C. A.; Xu, X. P.; Spengler, J. D.; Ware, J. H.; Fay, M. E.; Ferris, B. G.; Speizer, F. E. An association between air-pollution and mortality in 6 United-States cities. *N. Engl. J. Med.* **1993**, 329, 1753–1759.
- (2) Davidson, C. I.; Phalen, R. F.; Solomon, P. A. Airborne particulate matter and human health: A review. *Aerosol Sci. Technol.* **2005**, *39*, 737–749.
- (3) Pope, C. A.; Dockery, D. W. Health Effects of Fine Particulate Air Pollution: Lines That Connect. *J. Air Waste Manage. Assoc.* **2006**, 56, 709–742.
- (4) Kampa, M.; Castanas, E. Human Health Effects of Air Pollution. *Environ. Pollut.* **2008**, *151*, 362–367.
- (5) Falcon-Rodriguez, C. I.; Osornio-Vargas, A. R.; Sada-Ovalle, I.; Segura-Medina, P. Aeroparticles, Composition, and Lung Diseases. *Front. Immunol.* **2016**, *7*, 3.
- (6) Cohen, A. J.; Brauer, M.; Burnett, R.; Anderson, H. R.; Frostad, J.; Estep, K.; Balakrishnan, K.; Brunekreef, B.; Dandona, L.; Dandona, R.; Feigin, V.; Freedman, G.; Hubbell, B.; Jobling, A.; Kan, H.; Knibbs, L.; Liu, Y.; Martin, R.; Morawska, L.; Pope, C. A., III; Shin, H.; Straif, K.; Shaddick, G.; Thomas, M.; van Dingenen, R.; van Donkelaar, A.; Vos, T.; Murray, C. J. L.; Mohammad H Forouzanfar, M. H. Estimates and 25-Year Trends of the Global Burden of Disease Attributable to Ambient Air Pollution: An Analysis of Data from the Global Burden of Diseases Study 2015. *Lancet* 2017, 389, 1907—1918.
- (7) World Health Organization: AAP air quality database, available at: http://www.who.int/phe/health\_topics/outdoorair/databases/cities/en/, 2016 (last accessed in 03/2020).
- (8) Apte, J. S.; Brauer, M.; Cohen, A. J.; Ezzati, M.; Pope, C. A. Ambient PM<sub>2.5</sub> Reduces Global and Regional Life Expectancy. *Environ. Sci. Technol. Lett.* **2018**, *5*, 546–551.
- (9) United Nations: World urbanization prospects, available at: https://population.un.org/wup/, 2018 (last accessed in 03/2020).
- (10) Balakrishnan, K.; Dey, S.; Gupta, T.; Dhaliwal, R. S.; Brauer, M.; Cohen, A. J.; Stanaway, J. D.; Beig, G.; Joshi, T. K.; Aggarwal, A. N.; et al. The Impact of Air Pollution on Deaths, Disease Burden, and Life Expectancy across the States of India: The Global Burden of Disease Study 2017. *Lancet Planet. Heal.* **2019**, 3, e26–e39.
- (11) Baig, N. A.; Yawar, M.; Jain, K.; Singh, G.; Singh, S.; Siddharthan, D.; Habib, G. Association between Traffic Emissions Mixed with Resuspended Dust and Heart Rate Variability among Healthy Adults in Delhi. *Air Qual. Atmos. Heal.* **2020**, *13*, 371–378.
- (12) Haywood, J.; Boucher, O. Estimates of the Direct and Indirect Radiative Forcing Due to Tropospheric Aerosols: A Review. *Rev. Geophys.* **2000**, *38*, 513–543.
- (13) Seinfeld, J. H.; Pandis, S. N. Atmospheric Chemistry and Physics. In *From Air Pollution to Climate Change*, 2nd ed.; J. Wiley: New Jersey, 2006.
- (14) Hallquist, M.; Wenger, J. C.; Baltensperger, U.; Rudich, Y.; Simpson, D.; Claeys, M.; Dommen, J.; Donahue, N. M.; George, C.; Goldstein, A. H.; Hamilton, J. F.; Herrmann, H.; Hoffmann, T.; Iinuma, Y.; Jang, M.; Jenkin, M. E.; Jimenez, J. L.; Kiendler-Scharr, A.; Maenhaut, W.; McFiggans, G.; Mentel, T. F.; Monod, A.; Prévôt, A. S. H.; Seinfeld, J. H.; Surratt, J. D.; Szmigielski, R.; Wildt, J. The Formation, Properties and Impact of Secondary Organic Aerosol: Current and Emerging Issues. Atmos. Chem. Phys. 2009, 9, 5155–5236.
- (15) Presto, A. A.; Miracolo, M. A.; Kroll, J. H.; Worsnop, D. R.; Robinson, A. L.; Donahue, N. M. Intermediate-Volatility Organic Compounds: A Potential Source of Ambient Oxidized Organic Aerosol. *Environ. Sci. Technol.* **2009**, *43*, 4744–4749.
- (16) Shrivastava, M.; Cappa, C. D.; Fan, J.; Goldstein, A. H.; Guenther, A. B.; Jimenez, J. L.; Kuang, C.; Laskin, A.; Martin, S. T.; Ng, N. L.; Petaja, T.; Pierce, J. R.; Rasch, P. J.; Roldin, P.; Seinfeld, J. H.; Shilling, J.; Smith, J. N.; Thornton, J. A.; Volkamer, R.; Wang, J.; Worsnop, D. R.; Zaveri, R. A.; Zelenyuk, A.; Zhang, Q. Recent Advances in Understanding Secondary Organic Aerosol: Implications for Global Climate Forcing. *Rev. Geophys.* 2017, 55, 509–559.

- (17) Robinson, A. L.; Donahue, N. M.; Shrivastava, M. K.; Weitkamp, E. A.; Sage, A. M.; Grieshop, A. P.; Lane, T. E.; Pierce, J. R.; Pandis, S. N. Rethinking Organic Aerosols: Semivolatile Emissions and Photochemical Aging. Science 2007, 315, 1259-1262. (18) Jimenez, J. L.; Canagaratna, M. R.; Donahue, N. M.; Prevot, A. S. H.; Zhang, Q.; Kroll, J. H.; DeCarlo, P. F.; Allan, J. D.; Coe, H.; Ng, N. L.; Aiken, A. C.; Docherty, K. S.; Ulbrich, I. M.; Grieshop, A. P.; Robinson, A. L.; Duplissy, J.; Smith, J. D.; Wilson, K. R.; Lanz, V. A.; Hueglin, C.; Sun, Y. L.; Tian, J.; Laaksonen, A.; Raatikainen, T.; Rautiainen, J.; Vaattovaara, P.; Ehn, M.; Kulmala, M.; Tomlinson, J. M.; Collins, D. R.; Cubison, M. J.; Dunlea, E. J.; Huffman, J. A.; Onasch, T. B.; Alfarra, M. R.; Williams, P. I.; Bower, K.; Kondo, Y.; Schneider, J.; Drewnick, F.; Borrmann, S.; Weimer, S.; Demerjian, K.; Salcedo, D.; Cottrell, L.; Griffin, R.; Takami, A.; Miyoshi, T.; Hatakeyama, S.; Shimono, A.; Sun, J. Y.; Zhang, Y. M.; Dzepina, K.; Kimmel, J. R.; Sueper, D.; Jayne, J. T.; Herndon, S. C.; Trimborn, A. M.; Williams, L. R.; Wood, E. C.; Middlebrook, A. M.; Kolb, C. E.; Baltensperger, U.; Worsnop, D. R. Evolution of Organic Aerosols in the Atmosphere. Science 2009, 326, 1525-1529.
- (19) Zhang, Q.; Jimenez, J. L.; Canagaratna, M. R.; Allan, J. D.; Coe, H.; Ulbrich, I.; Alfarra, M. R.; Takami, A.; Middlebrook, A. M.; Sun, Y. L.; Dzepina, K.; Dunlea, E.; Docherty, K.; DeCarlo, P. F.; Salcedo, D.; Onasch, T.; Jayne, J. T.; Miyoshi, T.; Shimono, A.; Hatakeyama, S.; Takegawa, N.; Kondo, Y.; Schneider, J.; Drewnick, F.; Borrmann, S.; Weimer, S.; Demerjian, K.; Williams, P.; Bower, K.; Bahreini, R.; Cottrell, L.; Griffin, R. J.; Rautiainen, J.; Sun, J. Y.; Zhang, Y. M.; Worsnop, D. R. Ubiquity and dominance of oxygenated species in organic aerosols in anthropogenically-influenced Northern Hemisphere midlatitudes. *Geophys. Res. Lett.* 2007, 34 (13), No. L13801.
- (20) Goldstein, A. H.; Galbally, I. E. Known and Unexplored Organic Constituents in the Earth's Atmosphere. *Environ. Sci. Technol.* **2007**, *41*, 1514–1521.
- (21) Heald, C. L.; Jacob, D. J.; Park, R. J.; Russell, L. M.; Huebert, B. J.; Seinfeld, J. H.; Liao, H.; Weber, R. J. A Large Organic Aerosol Source in the Free Troposphere Missing from Current Models. *Geophys. Res. Lett.* **2005**, 32 (18), No. L18809.
- (22) Volkamer, R.; Jimenez, J. L.; Martini, F. S.; Dzepina, K.; Zhang, Q.; Salcedo, D.; Molina, L. T.; Worsnop, D. R.; Molina, M. J. Secondary Organic Aerosol Formation from Anthropogenic Air Pollution: Rapid and Higher than Expected. *Geophys. Res. Lett.* **2006**, 33 (17), No. L17811.
- (23) Tandon, A.; Yadav, S.; Attri, A. K. Coupling between Meteorological Factors and Ambient Aerosol Load. *Atmos. Environ.* **2010**, *44*, 1237–1243.
- (24) Jaiprakash Singhai, A.; Habib, G.; Raman, R. S.; Gupta, T. Chemical Characterization of PM<sub>1.0</sub> Aerosol in Delhi and Source Apportionment Using Positive Matrix Factorization. *Environ. Sci. Pollut. Res.* **2017**, 24, 445–462.
- (25) Pant, P.; Harrison, R. M. Critical Review of Receptor Modelling for Particulate Matter: A Case Study of India. *Atmos. Environ.* **2012**, 49, 1–12.
- (26) Chowdhury, S.; Dey, S.; Guttikunda, S.; Pillarisetti, A.; Smith, K. R.; Di Girolamo, L. Indian Annual Ambient Air Quality Standard Is Achievable by Completely Mitigating Emissions from Household Sources. *Proc. Natl. Acad. Sci. U.S.A.* **2019**, *116*, 10711–10716.
- (27) Guttikunda, S. K.; Calori, G. A GIS Based Emissions Inventory at 1 Km × 1 Km Spatial Resolution for Air Pollution Analysis in Delhi, India. *Atmos. Environ.* **2013**, *67*, 101–111.
- (28) Rai, P.; Furger, M.; El, I.; Kumar, V.; Wang, L.; Singh, A.; Dixit, K.; Bhattu, D.; Petit, J.; Ganguly, D.; Rastogi, N.; Baltensperger, U.; Tripathi, S. N.; Slowik, S. N.; Prévôt, A. S. H. Real-Time Measurement and Source Apportionment of Elements in Delhi's Atmosphere. *Sci. Total Environ.* **2020**, *742*, No. 140332.
- (29) Saikawa, E.; Wu, Q.; Zhong, M.; Avramov, A.; Ram, K.; Stone, E. A.; Stockwell, C. E.; Jayarathne, T.; Panday, A. K.; Yokelson, R. J. Garbage Burning in South Asia: How Important Is It to Regional Air Quality? *Environ. Sci. Technol.* **2020**, *54*, 9928–9938.
- (30) Hama, S. M. L.; Kumar, P.; Harrison, R. M.; Bloss, W. J.; Khare, M.; Mishra, S.; Namdeo, A.; Sokhi, R.; Goodman, P.; Sharma, C.

- Four-Year Assessment of Ambient Particulate Matter and Trace Gases in the Delhi-NCR Region of India. *Sustainable Cities Soc.* **2020**, *54*, No. 102003.
- (31) Bhandari, S.; Gani, S.; Patel, K.; Wang, D. S.; Soni, P.; Arub, Z.; Habib, G.; Apte, J. S.; Hildebrandt Ruiz, L. Sources and Atmospheric Dynamics of Organic Aerosol in New Delhi, India: Insights from Receptor Modeling. *Atmos. Chem. Phys.* **2020**, *20*, 735–752.
- (32) Gani, S.; Bhandari, S.; Seraj, S.; Wang, D. S.; Patel, K.; Soni, P.; Arub, Z.; Habib, G.; Hildebrandt Ruiz, L.; Apte, J. S. Submicron Aerosol Composition in the World's Most Polluted Megacity: The Delhi Aerosol Supersite Study. *Atmos. Chem. Phys.* **2019**, *19*, 6843–6859.
- (33) Badarinath, K. V. S.; Kiran Chand, T. R.; Krishna Prasad, V. Agriculture Crop Residue Burning in the Indo-Gangetic Plains A Study Using IRS-P6 AWiFS Satellite Data. *Curr. Sci.* **2006**, *91*, 1085–1089
- (34) Cusworth, D. H.; Mickley, L. J.; Sulprizio, M. P.; Liu, T.; Marlier, M. E.; Defries, R. S.; Guttikunda, S. K.; Gupta, P. Quantifying the Influence of Agricultural Fires in Northwest India on Urban Air Pollution in Delhi, India. *Environ. Res. Lett.* **2018**, *13*, 044018.
- (35) Kulkarni, S. H.; Ghude, S. D.; Jena, C.; Karumuri, R. K.; Sinha, B.; Sinha, V.; Kumar, R.; Soni, V. K.; Khare, M. How Much Does Large-Scale Crop Residue Burning Affect the Air Quality in Delhi? *Environ. Sci. Technol.* **2020**, *54*, 4790–4799.
- (36) Pant, P.; Shukla, A.; Kohl, S. D.; Chow, J. C.; Watson, J. G.; Harrison, R. M. Characterization of Ambient PM<sub>2.5</sub> at a Pollution Hotspot in New Delhi, India and Inference of Sources. *Atmos. Environ.* **2015**, *109*, 178–189.
- (37) Guttikunda, S. K.; Gurjar, B. R. Role of Meteorology in Seasonality of Air Pollution in Megacity Delhi, India. *Environ. Monit. Assess.* **2012**, *184*, 3199–3211.
- (38) Yadav, S.; Tandon, A.; Attri, A. K. Characterization of Aerosol Associated Non-Polar Organic Compounds Using TD-GC-MS: A Four Year Study from Delhi, India. *J. Hazard. Mater.* **2013**, 252–253, 29–44.
- (39) Trivedi, D. K.; Ali, K.; Beig, G. Impact of Meteorological Parameters on the Development of Fine and Coarse Particles over Delhi. *Sci. Total Environ.* **2014**, 478, 175–183.
- (40) Badarinath, K. V. S.; Kumar Kharol, S.; Rani Sharma, A. Longrange transport of aerosols from agriculture crop residue burning in Indo-Gangetic Plains-A study using LIDAR, ground measurements and satellite data. *J. Atmos. Sol.-Terr. Phys.* **2009**, *71*, 112–120.
- (41) Perrino, C.; Tiwari, S.; Catrambone, M.; Torre, S. D.; Rantica, E.; Canepari, S. Chemical Characterization of Atmospheric PM in Delhi, India, during Different Periods of the Year Including Diwali Festival. *Atmos. Pollut. Res.* **2011**, *2*, 418–427.
- (42) Tiwari, S.; Chate, D. M.; Srivastava, M. K.; Safai, P. D.; Srivastava, A. K.; Bisht, D. S.; Padmanabhamurty, B. Statistical Evaluation of PM<sub>10</sub> and Distribution of PM<sub>1</sub>, PM<sub>2.5</sub>, and PM<sub>10</sub> in Ambient Air Due to Extreme Fireworks Episodes (Deepawali Festivals) in Megacity Delhi. *Nat. Hazard.* **2012**, *61*, 521–531.
- (43) Ng, N. L.; Herndon, S. C.; Trimborn, A.; Canagaratna, M. R.; Croteau, P. L.; Onasch, T. B.; Sueper, D.; Worsnop, D. R.; Zhang, Q.; Sun, Y. L.; Jayne, J. T. An Aerosol Chemical Speciation Monitor (ACSM) for Routine Monitoring of the Composition and Mass Concentrations of Ambient Aerosol. *Aerosol Sci. Technol.* **2011**, *45*, 780–794.
- (44) Drinovec, L.; Močnik, G.; Zotter, P.; Prévôt, A. S. H.; Ruckstuhl, C.; Coz, E.; Rupakheti, M.; Sciare, J.; Müller, T.; Wiedensohler, A.; Hansen, A. D. A. The "Dual-Spot" Aethalometer: An Improved Measurement of Aerosol Black Carbon with Real-Time Loading Compensation. *Atmos. Meas. Tech.* **2015**, *8*, 1965–1979.
- (45) Hussein, T.; Dal Maso, M.; Petäjä, T.; Koponen, I. K.; Paatero, P.; Aalto, P. P.; Hämeri, K.; Kulmala, M. Evaluation of an Automatic Algorithm for Fitting the Particle Number Size Distributions. *Boreal Environ. Res.* **2005**, *10*, 337–355.
- (46) Sandradewi, J.; Prévôt, A. S. H.; Szidat, S.; Perron, N.; Alfarra, M. R.; Lanz, V. A.; Weingartner, E.; Baltensperger, U. R. S. Using Aerosol Light Abosrption Measurements for the Quantitative

- Determination of Wood Burning and Traffic Emission Contribution to Particulate Matter. *Environ. Sci. Technol.* **2008**, *42*, 3316–3323.
- (47) Ulbrich, I. M.; Canagaratna, M. R.; Zhang, Q.; Worsnop, D. R.; Jimenez, J. L. Interpretation of Organic Components from Positive Matrix Factorization of Aerosol Mass Spectrometric Data. *Atmos. Chem. Phys.* **2009**, *9*, 2891.
- (48) Zhang, Q.; Jimenez, J. L.; Canagaratna, M. R.; Ulbrich, I. M.; Ng, N. L.; Worsnop, D. R.; Sun, Y. Understanding Atmospheric Organic Aerosols via Factor Analysis of Aerosol Mass Spectrometry: A Review. *Anal. Bioanal. Chem.* **2011**, *401*, 3045–3067.
- (49) Sun, Y. L.; Zhang, Q.; Schwab, J. J.; Yang, T.; Ng, N. L.; Demerjian, K. L. Factor Analysis of Combined Organic and Inorganic Aerosol Mass Spectra from High Resolution Aerosol Mass Spectrometer Measurements. *Atmos. Chem. Phys.* **2012**, *12*, 8537–8551
- (50) Sun, Y. L.; Wang, Z. F.; Fu, P. Q.; Yang, T.; Jiang, Q.; Dong, H. B.; Li, J.; Jia, J. J. Aerosol Composition, Sources and Processes during Wintertime in Beijing, China. *Atmos. Chem. Phys.* **2013**, *13*, 4577–4502
- (51) Ng, N. L.; Canagaratna, M. R.; Zhang, Q.; Jimenez, J. L.; Tian, J.; Ulbrich, I. M.; Kroll, J. H.; Docherty, K. S.; Chhabra, P. S.; Bahreini, R.; Murphy, S. M.; Seinfeld, J. H.; Hildebrandt, L.; Donahue, N. M.; Decarlo, P. F.; Lanz, V. A.; Prévôt, A. S. H.; Dinar, E.; Rudich, Y.; Worsnop, D. R. Organic Aerosol Components Observed in Northern Hemispheric Datasets from Aerosol Mass Spectrometry. *Atmos. Chem. Phys.* **2010**, *10*, 4625–4641.
- (52) Elser, M.; Huang, R. J.; Wolf, R.; Slowik, J. G.; Wang, Q.; Canonaco, F.; Li, G.; Bozzetti, C.; Daellenbach, K. R.; Huang, Y.; Zhang, R.; Li, Z.; Cao, J.; Baltensperger, U.; El-Haddad, I.; Prévôt, A. S. H. New Insights into PM<sub>2.5</sub> Chemical Composition and Sources in Two Major Cities in China during Extreme Haze Events Using Aerosol Mass Spectrometry. *Atmos. Chem. Phys.* **2016**, *16*, 3207–3225.
- (53) Lanz, V. A.; Alfarra, M. R.; Baltensperger, U.; Buchmann, B.; Hueglin, C.; Prévôt, A. S. H. Source Apportionment of Submicron Organic Aerosols at an Urban Site by Factor Analytical Modelling of Aerosol Mass Spectra. *Atmos. Chem. Phys.* **2007**, *7*, 1503–1522.
- (54) Hildebrandt, L.; Engelhart, G. J.; Mohr, C.; Kostenidou, E.; Lanz, V. A.; Bougiatioti, A.; Decarlo, P. F.; Prevot, A. S. H.; Baltensperger, U.; Mihalopoulos, N.; Donahue, N. M.; Pandis, S. N. Aged Organic Aerosol in the Eastern Mediterranean: The Finokalia Aerosol Measurement Experiment-2008. *Atmos. Chem. Phys.* **2010**, *10*, 4167–4186.
- (55) Dai, Q.; Schulze, B. C.; Bi, X.; Bui, A. A. T.; Guo, F.; Wallace, H. W.; Sanchez, N. P.; Flynn, J. H.; Lefer, B. L.; Feng, Y.; Griffin, R. J. Seasonal Differences in Formation Processes of Oxidized Organic Aerosol near Houston, TX. Atmos. Chem. Phys. 2019, 19, 9641–9661.
- (56) Patel, K.; Wang, D.; Chhabra, P.; Bean, J.; Dhulipala, S. V.; Hildebrandt Ruiz, L. Effects of Sources and Meteorology on Ambient Particulate Matter in Austin, Texas. ACS Earth Space Chem. **2020**, *4*, 602–613.
- (57) Xu, L.; Suresh, S.; Guo, H.; Weber, R. J.; Ng, N. L. Aerosol Characterization over the Southeastern United States Using High-Resolution Aerosol Mass Spectrometry: Spatial and Seasonal Variation of Aerosol Composition and Sources with a Focus on Organic Nitrates. *Atmos. Chem. Phys.* **2015**, *15*, 7307–7336.
- (58) Mohr, C.; Huffman, J. A.; Cubison, M. J.; Aiken, A. C.; Docherty, K. S.; Kimmel, J. R.; Ulbrich, I. M.; Hannigan, M.; Jimenez, J. L. Characterization of Primary Organic Aerosol Emissions from Meat Cooking, Trash Burning, and Motor Vehicles with High-Resolution Aerosol Mass Spectrometry and Comparison with Ambient and Chamber Observations. *Environ. Sci. Technol.* 2009, 43, 2443–2449.
- (59) Aiken, A. C.; Salcedo, D.; Cubison, M. J.; Huffman, J. A.; DeCarlo, P. F.; Ulbrich, I. M.; Docherty, K. S.; Sueper, D.; Kimmel, J. R.; Worsnop, D. R.; Trimborn, A.; Northway, M.; Stone, E. A.; Schauer, J. J.; Volkamer, R. M.; Fortner, E.; De Foy, B.; Wang, J.; Laskin, A.; Shutthanandan, V.; Zheng, J.; Zhang, R.; Gaffney, J.; Marley, N. A.; Paredes-Miranda, G.; Arnott, W. P.; Molina, L. T.;

- Sosa, G.; Jimenez, J. L. Mexico City Aerosol Analysis during MILAGRO Using High Resolution Aerosol Mass Spectrometry at the Urban Supersite (T0) Part 1: Fine Particle Composition and Organic Source Apportionment. *Atmos. Chem. Phys.* **2009**, *9*, 6633–6653.
- (60) Xing, L.; Wu, J.; Elser, M.; Tong, S.; Liu, S.; Li, X.; Liu, L.; Cao, J.; Zhou, J.; El-Haddad, I.; Huang, R.; Ge, M.; Tie, X.; Prévôt, A. S. H.; Li, G. Wintertime Secondary Organic Aerosol Formation in Beijing-Tianjin-Hebei (BTH): Contributions of HONO Sources and Heterogeneous Reactions. *Atmos. Chem. Phys.* **2019**, *19*, 2343–2359.
- (61) Paatero, P.; Tapper, U. Positive Matrix Factorization: A Nonnegative Factor Model with Optimal Utilization of Error Estimates of Data Values. *Environmetrics* **1994**, *5*, 111–126.
- (62) Sun, Y.; Wang, Z.; Dong, H.; Yang, T.; Li, J.; Pan, X.; Chen, P.; Jayne, J. T. Characterization of Summer Organic and Inorganic Aerosols in Beijing, China with an Aerosol Chemical Speciation Monitor. *Atmos. Environ.* **2012**, *51*, 250–259.
- (63) Ng, N. L.; Canagaratna, M. R.; Jimenez, J. L.; Zhang, Q.; Ulbrich, I. M.; Worsnop, D. R. Real-Time Methods for Estimating Organic Component Mass Concentrations from Aerosol Mass Spectrometer Data. *Environ. Sci. Technol.* **2011**, *45*, 910–916.
- (64) Gelaro, R.; McCarty, W.; Suárez, M. J.; Todling, R.; Molod, A.; Takacs, L.; Randles, C. A.; Darmenov, A.; Bosilovich, M. G.; Reichle, R.; Wargan, K.; Coy, L.; Cullather, R.; Draper, C.; Akella, S.; Buchard, V.; Conaty, A.; da Silva, A. M.; Gu, W.; Kim, G. K.; Koster, R.; Lucchesi, R.; Merkova, D.; Nielsen, J. E.; Partyka, G.; Pawson, S.; Putman, W.; Rienecker, M.; Schubert, S. D.; Sienkiewicz, M.; Zhao, B. The Modern-Era Retrospective Analysis for Research and Applications, Version 2 (MERRA-2). *J. Climate* 2017, 30, 5419–5454.
- (65) Justice, C. O.; Vermote, E.; Townshend, J. R. G.; Defries, R.; Roy, D. P.; Hall, D. K.; Salomonson, V. V.; Privette, J. L.; Riggs, G.; Strahler, A.; Lucht, W.; Myneni, R. B.; Knyazikhin, Y.; Running, S. W.; Nemani, R. R.; Wan, Z.; Huete, A. R.; Van Leeuwen, W.; Wolfe, R. E.; Giglio, L.; Muller, J. P.; Lewis, P.; Barnsley, M. J. The Moderate Resolution Imaging Spectroradiometer (MODIS): Land Remote Sensing for Global Change Research. *IEEE Trans. Geosci. Remote Sens.* 1998, 36, 1228–1249.
- (66) Giglio, L.; Schroeder, W.; Justice, C. O. The Collection 6 MODIS Active Fire Detection Algorithm and Fire Products. *Remote Sens. Environ.* **2016**, *178*, 31–41.
- (67) Fire Information for Resource Management System (FIRMS), available at: https://earthdata.nasa.gov/earth-observation-data/near-real-time/firms, last accessed in 08/2020.
- (68) Petit, J. E.; Favez, O.; Albinet, A.; Canonaco, F. A User-Friendly Tool for Comprehensive Evaluation of the Geographical Origins of Atmospheric Pollution: Wind and Trajectory Analyses. *Environ. Model. Softw.* **2017**, *88*, 183–187.
- (69) Henry, R.; Norris, G. A.; Vedantham, R.; Turner, J. R. Source Region Identification Using Kernel Smoothing. *Environ. Sci. Technol.* **2009**, 43, 4090–4097.
- (70) Salcedo, D.; Onasch, T. B.; Dzepina, K.; Canagaratna, M. R.; Zhang, Q.; Huffmann, J. A.; DeCarlo, P. F.; Jayne, J. T.; Mortimer, P.; Worsnop, D. R.; Kolb, C. E.; Johnson, K. S.; Zuberi, B.; Marr, L. C.; Volkamer, R.; Molina, L. T.; Molina, M. J.; Cardenas, B.; Bernabé, R. M.; Márquez, C.; Gaffney, J. S.; Marley, N. A.; Laskin, A.; Shutthanandan, V.; Xie, Y.; Brune, W.; Lesher, R.; Shirley, T.; Jimenez, J. L. Characterization of Ambient Aerosols in Mexico City during the MCMA-2003 Campaign with Aerosol Mass Spectrometry: Results from the CENICA Supersite. *Atmos. Chem. Phys.* **2006**, *6*, 925–946.
- (71) Jiang, Q.; Sun, Y. L.; Wang, Z.; Yin, Y. Aerosol Composition and Sources during the Chinese Spring Festival: Fireworks, Secondary Aerosol, and Holiday Effects. *Atmos. Chem. Phys.* **2015**, *15*, 6023–6034.
- (72) Gani, S.; Bhandari, S.; Patel, K.; Seraj, S.; Soni, P.; Arub, Z.; Habib, G.; Hildebrandt Ruiz, L.; Apte, J. S. Particle Number Concentrations and Size Distribution in a Polluted Megacity: The Delhi Aerosol Supersite Study. *Atmos. Chem. Phys.* **2020**, 20, 8533–8549.

- (73) Norris, G.; Duvall, R.; Brown, S.; Bai, S. EPA Positive M Atrix Factorization (PMF) 5.0 Fundamentals and User Guide, 2015. https://www.epa.gov/sites/production/files/2015-02/documents/pmf 5.0 user guide.pdf (last accessed in 05/2020).
- (74) Petit, J. E.; Favez, O.; Sciare, J.; Canonaco, F.; Croteau, P.; Močnik, G.; Jayne, J.; Worsnop, D.; Leoz-Garziandia, E. Submicron Aerosol Source Apportionment of Wintertime Pollution in Paris, France by Double Positive Matrix Factorization (PMF2) Using an Aerosol Chemical Speciation Monitor (ACSM) and a Multi-Wavelength Aethalometer. *Atmos. Chem. Phys.* **2014**, *14*, 13773–13787.
- (75) Allan, J. D.; Williams, P. I.; Morgan, W. T.; Martin, C. L.; Flynn, M. J.; Lee, J.; Nemitz, E.; Phillips, G. J.; Gallagher, M. W.; Coe, H. Contributions from Transport, Solid Fuel Burning and Cooking to Primary Organic Aerosols in Two UK Cities. *Atmos. Chem. Phys.* **2010**, *10*, 647–668.
- (76) He, L. Y.; Lin, Y.; Huang, X. F.; Guo, S.; Xue, L.; Su, Q.; Hu, M.; Luan, S. J.; Zhang, Y. H. Characterization of High-Resolution Aerosol Mass Spectra of Primary Organic Aerosol Emissions from Chinese Cooking and Biomass Burning. *Atmos. Chem. Phys.* **2010**, *10*, 11535–11543.
- (77) Reyes Villegas, E.; Bannan, T. J.; Le Breton, M.; Mehra, A.; Priestley, M.; Percival, C.; Coe, H.; Allan, J. Online Chemical Characterization of Food Cooking Organic Aerosols: Implications for Source Apportionment. *Environ. Sci. Technol.* **2018**, *52*, 5308–5318.
- (78) Mohr, C.; DeCarlo, P. F.; Heringa, M. F.; Chirico, R.; Slowik, J. G.; Richter, R.; Reche, C.; Alastuey, A.; Querol, X.; Seco, R.; Peñuelas, J.; Jimenez, J. L.; Crippa, M.; Zimmermann, R.; Baltensperger, U.; Prévot, A. S. H. Identification and Quantification of Organic Aerosol from Cooking and Other Sources in Barcelona Using Aerosol Mass Spectrometer Data. *Atmos. Chem. Phys.* **2012**, *12*, 1649–1665.
- (79) Srivastava, D.; Favez, O.; Petit, J. E.; Zhang, Y.; Sofowote, U. M.; Hopke, P. K.; Bonnaire, N.; Perraudin, E.; Gros, V.; Villenave, E.; Albinet, A. Speciation of Organic Fractions Does Matter for Aerosol Source Apportionment. Part 3: Combining off-Line and on-Line Measurements. *Sci. Total Environ.* **2019**, *690*, 944–955.
- (80) Crippa, M.; Canonaco, F.; Lanz, V. A.; Äijälä, M.; Allan, J. D.; Carbone, S.; Capes, G.; Ceburnis, D.; Dall'Osto, M.; Day, D. A.; DeCarlo, P. F.; Ehn, M.; Eriksson, A.; Freney, E.; Ruiz, L. H.; Hillamo, R.; Jimenez, J. L.; Junninen, H.; Kiendler-Scharr, A.; Kortelainen, A. M.; Kulmala, M.; Laaksonen, A.; Mensah, A. A.; Mohr, C.; Nemitz, E.; O'Dowd, C.; Ovadnevaite, J.; Pandis, S. N.; Petäjä, T.; Poulain, L.; Saarikoski, S.; Sellegri, K.; Swietlicki, E.; Tiitta, P.; Worsnop, D. R.; Baltensperger, U.; Prévôt, A. S. H. Organic Aerosol Components Derived from 25 AMS Data Sets across Europe Using a Consistent ME-2 Based Source Apportionment Approach. *Atmos. Chem. Phys.* 2014, 14, 6159–6176.
- (81) Fang, Z.; Deng, W.; Zhang, Y.; Ding, X.; Tang, M.; Liu, T.; Hu, Q.; Zhu, M.; Wang, Z.; Yang, W.; Huang, Z.; Song, W.; Bi, X.; Chen, J.; Sun, Y.; George, C.; Wang, X. Open Burning of Rice, Corn and Wheat Straws: Primary Emissions, Photochemical Aging, and Secondary Organic Aerosol Formation. *Atmos. Chem. Phys.* **2017**, 17, 14821–14839.
- (82) Cubison, M. J.; Ortega, A. M.; Hayes, P. L.; Farmer, D. K.; Day, D.; Lechner, M. J.; Brune, W. H.; Apel, E.; Diskin, G. S.; Fisher, J. A.; Fuelberg, H. E.; Hecobian, A.; Knapp, D. J.; Mikoviny, T.; Riemer, D.; Sachse, G. W.; Sessions, W.; Weber, R. J.; Weinheimer, A. J.; Wisthaler, A.; Jimenez, J. L. Effects of Aging on Organic Aerosol from Open Biomass Burning Smoke in Aircraft and Laboratory Studies. *Atmos. Chem. Phys.* **2011**, *11*, 12049–12064.
- (83) Farmer, D. K.; Matsunaga, A.; Docherty, K. S.; Surratt, J. D.; Seinfeld, J. H.; Ziemann, P. J.; Jimenez, J. L. Response of an Aerosol Mass Spectrometer to Organonitrates and Organosulfates and Implications for Atmospheric Chemistry. *Proc. Natl. Acad. Sci. U.S.A.* **2010**, *107*, *6670*–*6675*.
- (84) Ineichen, H.; Berger, B. Pyrotechnics in Fireworks. *Chimia* **2004**, *58*, 369–373.

- (85) Kumar, P.; Kumar, R.; Yadav, S. Water-Soluble Ions and Carbon Content of Size-Segregated Aerosols in New Delhi, India: Direct and Indirect Influences of Firework Displays. *Environ. Sci. Pollut. Res.* **2016**, 23, 20749–20760.
- (86) Hu, W.; Campuzano-Jost, P.; Day, D. A.; Croteau, P.; Canagaratna, M. R.; Jayne, J. T.; Worsnop, D. R.; Jimenez, J. L. Evaluation of the New Capture Vaporizer for Aerosol Mass Spectrometers (AMS) through Field Studies of Inorganic Species. *Aerosol Sci. Technol.* **2017**, *51*, 735–754.
- (87) Song, S.; Gao, M.; Xu, W.; Sun, Y.; Worsnop, D. R.; Jayne, J. T.; Zhang, Y.; Zhu, L.; Li, M.; Zhou, Z.; Cheng, C.; Lv, Y.; Wang, Y.; Xu, X.; Lin, N.; Wang, Y.; Wang, S.; Munger, J. W.; Jacob, D.; Mcelroy, M. B.; et al. Possible Heterogeneous Hydroxymethanesulfonate (HMS) Chemistry in Northern China Winter Haze. *Atmos. Chem. Phys.* **2019**, *19*, 1357–1371.
- (88) Slowik, J. G.; Stroud, C.; Bottenheim, J. W.; Brickell, P. C.; Chang, R. Y. W.; Liggio, J.; Makar, P. A.; Martin, R. V.; Moran, M. D.; Shantz, N. C.; Sjostedt, S. J.; Van Donkelaar, A.; Vlasenko, A.; Wiebe, H. A.; Xia, A. G.; Zhang, J.; Leaitch, W. R.; Abbatt, J. P. D. Characterization of a Large Biogenic Secondary Organic Aerosol Event from Eastern Canadian Forests. *Atmos. Chem. Phys.* **2010**, *10*, 2825–2845.
- (89) Fourtziou, L.; Liakakou, E.; Stavroulas, I.; Theodosi, C.; Zarmpas, P.; Psiloglou, B.; Sciare, J.; Maggos, T.; Bairachtari, K.; Bougiatioti, A.; Gerasopoulos, E.; Sarda-Estève, R.; Bonnaire, N.; Mihalopoulos, N. Multi-Tracer Approach to Characterize Domestic Wood Burning in Athens (Greece) during Wintertime. *Atmos. Environ.* **2017**, *148*, 89–101.
- (90) Li, J.; Song, Y.; Mao, Y.; Mao, Z.; Wu, Y.; Li, M.; Huang, X.; He, Q.; Hu, M. Chemical Characteristics and Source Apportionment of PM<sub>2.5</sub> during the Harvest Season in Eastern China's Agricultural Regions. *Atmos. Environ.* **2014**, *92*, 442–448.
- (91) Wang, D. S.; Ruiz, L. H. Secondary Organic Aerosol from Chlorine-Initiated Oxidation of Isoprene. *Atmos. Chem. Phys.* **2017**, 17, 13491–13508.
- (92) Goetz, J. D.; Giordano, M. R.; Stockwell, C. E.; Christian, T. J.; Maharjan, R.; Adhikari, S.; Bhave, P. V.; Praveen, P. S.; Panday, A. K.; Jayarathne, T.; Stone, E. A.; Yokelson, R. J.; Decarlo, P. F. Speciated Online PM<sub>1</sub> from South Asian Combustion Sources-Part 1: Fuel-Based Emission Factors and Size Distributions. *Atmos. Chem. Phys.* **2018**, *18*, 14653–14679.
- (93) Jayarathne, T.; Stockwell, C. E.; Christian, T. J.; Bhave, P. V.; Praveen, P. S.; Panday, A. K.; Adhikari, S.; Maharjan, R.; Goetz, J. D.; DeCarlo, P. F.; Saikawa, E.; Yokelson, R. J.; Stone, E. A.; et al. Nepal Ambient Monitoring and Source Testing Experiment (NAMaSTE): Emissions of Particulate Matter from Wood and Dung Cooking Fires, wood-and dung-fueled cooking fires, garbage and crop residue-burning, brick kilns, and other sources. *Atmos. Chem. Phys.* **2018**, *18*, 2259–2286.
- (94) Zhang, Y. J.; Tang, L. L.; Wang, Z.; Yu, H. X.; Sun, Y. L.; Liu, D.; Qin, W.; Canonaco, F.; Prévôt, A. S. H.; Zhang, H. L.; Zhou, H. C. Insights into Characteristics, Sources, and Evolution of Submicron Aerosols during Harvest Seasons in the Yangtze River Delta Region, China. Atmos. Chem. Phys. 2015, 15, 1331–1349.
- (95) Li, J.; Pósfai, M.; Hobbs, P. V.; Buseck, P. R. Individual Aerosol Particles from Biomass Burning in Southern Africa: 2. Compositions and Aging of Inorganic Particles. *J. Geophys. Res.: Atmos.* **2003**, *108*, 1–12.
- (96) Hays, M. D.; Fine, P. M.; Geron, C. D.; Kleeman, M. J.; Gullett, B. K. Open Burning of Agricultural Biomass: Physical and Chemical Properties of Particle-Phase Emissions. *Atmos. Environ.* **2005**, 39, 6747–6764.
- (97) Levin, E. J. T.; McMeeking, G. R.; Carrico, C. M.; Mack, L. E.; Kreidenweis, S. M.; Wold, C. E.; Moosmüller, H.; Arnott, W. P.; Hao, W. M.; Collett, J. L.; Malm, W. C. Biomass Burning Smoke Aerosol Properties Measured during Fire Laboratory at Missoula Experiments (FLAME). *J. Geophys. Res.* **2010**, *115* (D18), No. D18210.
- (98) Sun, Y.; Jiang, Q.; Xu, Y.; Ma, Y.; Zhang, Y.; Liu, X.; Li, W.; Wang, F.; Li, J.; Wang, P.; Li, Z. Aerosol characterization over the

North China Plain: Haze lifecycle and biomass burning impacts in summer. *I. Geophys. Res.: Atmos.* **2016**, *121*, 2508–2521.

(99) Liu, J.; Zhang, X.; Parker, E. T.; Veres, P. R.; Roberts, J. M.; de Gouw, J. A.; Hayes, P. L.; Jimenez, J. L.; Murphy, J. G.; Ellis, R. A.; Huey, L. G.; Weber, R. J. On the gas-particle partitioning of soluble organic aerosol in two urban atmospheres with contrasting emissions: 2. Gas and particle phase formic acid. *J. Geophys. Res.: Atmos.* **2012**, 117, 1–15.